Available online at www.sciencedirect.com
ScienceDirect
Journal of Molecular Catalysis A: Chemical 259 (2006) 245–252
JOURNAL OF MOLECULAR CATALYSIS A: CHEMICAL
www.elsevier.com/locate/molcata

Preparation, characterization and catalytic behavior of SnO_2 supported Au catalysts for low-temperature CO oxidation

Shurong Wang, Jing Huang, Yingqiang Zhao, Shuping Wang, Xiaoying Wang, Tongying Zhang, Shihua Wu *, Shoumin Zhang, Weiping Huang

Department of Chemistry, Nankai University, Tianjin 300071, China

Received 23 April 2006; received in revised form 8 June 2006; accepted 9 June 2006
Available online 1 August 2006

Abstract

SnO_2 nanocrystals were synthesized by a precipitation process and then used as the support for Au/SnO_2 catalysts preparation via a deposition–precipitation method. The samples were characterized by means of X-ray diffraction (XRD), high-resolution transmission electron microscopy (HRTEM)/energy-dispersive X-ray spectra (EDS) and X-ray photoelectron spectroscopy (XPS). The influence of calcination temperature of SnO_2 support, calcination temperature of Au/SnO_2 catalysts and Au loading on the catalytic activity of Au/SnO_2 catalysts was investigated. The SnO_2 samples calcined at 573 and 673 K were found to be the suitable support materials for Au/SnO_2 catalysts. In all investigated Au/SnO_2 catalysts with different Au loading from 0.36 to 5.00 wt.%, the catalytic activity of the catalyst with 2.86 wt.% Au loading was the highest. The optimum calcination temperature of the Au/SnO_2 catalysts was 473 K. According to XRD, HRTEM and XPS, the catalytic activity of the Au/SnO_2 catalysts was related to the particle size of gold and tin oxide support, the fraction of metallic state Au and the degree of crystallinity of tin dioxide support.

Keywords: Au/SnO_2 catalysts; Deposition–precipitation method; Low-temperature CO oxidation

1. Introduction

Compared with inert bulk gold, supported gold catalysts show a surprising high catalytic in many reactions, such as the reduction of nitrogen oxides [1,2], the epoxidation of propene [3,4], complete oxidation of hydrocarbons, hydrogenation, water–gas shift reaction [5–12] and the low-temperature oxidation of CO [13–17]. Since Haruta's report [18] of the remarkably high activity of supported gold catalysts for low-temperature CO oxidation, interest in the potential applications of supported gold catalysts has increased dramatically, along with research efforts to understand the origin of this surprising activity. Haruta et al. [15–17] discovered when gold was highly dispersed on semiconductor metal oxides such as TiO_2, α-Fe_2O_3 and Co_3O_4, it turns out to be highly active for the low-temperature catalytic oxidation of CO.

Although the catalytic activity of gold catalysts in the low-temperature CO oxidation has been intensively studied during the last decade, the catalytic activity of gold supported on SnO_2 has seldom been discussed. Due to the particular physical and chemical properties of nanosized tin dioxide, SnO_2 has covered a wide range of applications such as catalyst, catalytic support, gas sensor, rechargeable Li battery and optical electronic device [19–21]. In previous work, we had synthesized Au/SnO_2 catalysts by a co-precipitation process, and their catalytic activity for CO oxidation was also investigated [22]. But the catalytic activity was not very satisfactory. There has already been a general consensus that the preparation method, the synthesis parameters, pretreatment conditions and the choice of the support all exert a significant influence on the ultimate catalytic performance. To improve the catalytic activity of Au/SnO_2 catalysts, in this work, various Au/SnO_2 catalysts were prepared by a deposition–precipitation method, and the influence of the calcination temperature of SnO_2 support, calcination temperature of Au/SnO_2 catalysts and Au loading on catalytic activity was investigated. Several techniques, such as X-ray diffraction (XRD), high-resolution transmission electron microscopy

* Corresponding author. Tel.: +86 22 23505896; fax: +86 22 23502458.
E-mail address: shrwang@nankai.edu.cn (S. Wu).

1381-1169/$ – see front matter © 2006 Elsevier B.V. All rights reserved.
doi:10.1016/j.molcata.2006.06.021

(HRTEM) and X-ray photoelectron spectroscopy (XPS), were employed to study the structure and the CO oxidation property of Au/SnO_2 catalysts.

2. Experimental

2.1. Catalyst preparation

SnO_2 support was synthesized by a precipitation process using $SnCl_4{\cdot}5H_2O$ and NH_4OH. Under vigorous stirring, 1 mol/L NH_4OH aqueous solution was added drop-wise to a 0.25 mol/L $SnCl_4$ solution until the pH of the solution was 7. The suspension formed was stirred for 1 h and then centrifuged and washed several times with deionized water and ethanol alternatively until Cl^- could not be examined by 0.1 mol/L $AgNO_3$ aqueous solution, and then the sample was dried overnight in air at 353 K. The as-prepared material was ground and calcined in air at 473, 573, 673 and 773 K for 3 h, respectively.

Au/SnO_2 catalysts were prepared by a deposition–precipitation method. Under vigorous stirring, SnO_2 support was dispersed in $HAuCl_4$ solution. Over a period of 1 h, 1 mol/L NH_4OH aqueous solution was added drop-wise to the above resulting slurry under vigorous stirring until the pH of the slurry was 10. The mixture was stirred for another hour, then filtered and washed with deionized water and ethanol alternately. The samples were dried at room temperature for 2 h in air, followed by calcination at different temperatures in air for 3 h.

2.2. Measurement of catalytic activity

Catalytic activity tests were performed in a continuous-flow fixed-bed microreactor, using 100 mg catalyst powder. A stainless steel tube with an inner diameter of 8 mm was chosen as the reactor tube. The reaction gas mixture consisting of 1 vol.% CO balanced with air was passed through the catalyst bed at a total flow rate of 33.4 mL/min. A typical weight hourly space velocity (WHSV) was 20,040 mL h^{-1} g^{-1}. After 30 min under reaction conditions, the effluent gases were analyzed online by GC-508A gas chromatography. The activity was expressed by the degree of CO conversion.

2.3. Catalyst characterization

X-ray diffraction analyses were performed on D/MAX-RAX diffractometer operating at 40 kV and 100 mA, using Cu Kα radiation (scanning range 2θ: 20–75°). Diffraction peaks of crystalline phases were compared with those of standard compounds reported in the JCPDS Data File. High-resolution transmission electron microscopy was carried out on a Philips-T20ST electron microscope, operating at 200 kV.

X-ray photoelectron spectroscopy measurements were performed with a Perkin-Elmer PHI 5600 spectrophotometer with the Mg Kα radiation. The operating conditions were kept constant at 187.85 eV and 250.0 W. In order to subtract the surface charging effect, the C 1s peak has been fixed, in agreement with the literature, at a binding energy of 284.6 eV.

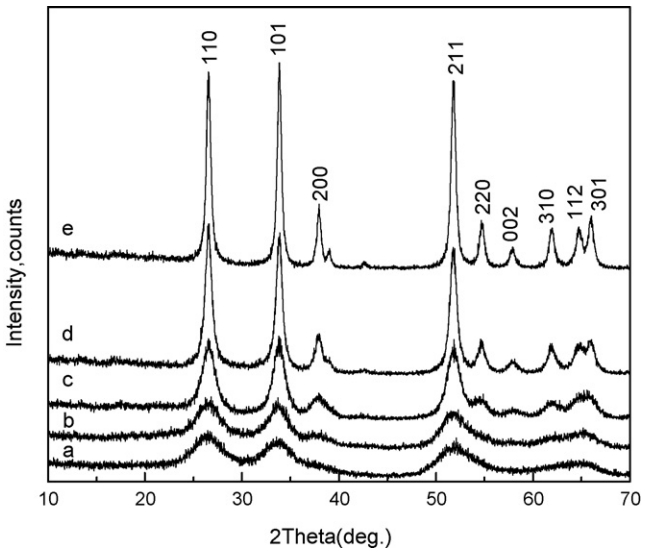

Fig. 1. XRD patterns of the SnO_2 samples calcined at different temperatures: 473 K (a), 573 K (b), 673 K (c), 773 K (d) and 873 K (e).

3. Results and discussion

3.1. Support and catalyst characterization

Fig. 1 shows the X-ray powder diffraction patterns of the as-prepared SnO_2 samples calcined at different temperatures. Compared to JCPDS (File No. 41-1445) standard pattern, the peaks agreed well with tetragonal rutile crystalline structure of SnO_2 crystal, with no additional lines belonging to other phases such as SnO, i.e. observed in any of the X-ray diffraction patterns. This indicated that the increase of calcination temperature did not cause the transformation of lattice structure of SnO_2. With the increase of calcination temperature, the intensity of diffraction peaks of [1 1 0], [1 0 1] and [2 1 1] crystal faces gradually increased, and diffraction peaks of [2 0 0], [2 2 0], [0 0 2], [3 1 0] and [3 0 1] crystal faces were gradually visible. This showed that crystalline structure of SnO_2 tended towards integrity. From the information provided by XRD patterns, we could see that the characterization diffraction peaks of the samples were apparently broad at low temperature (<673 K), showing that the small-sized nanocrystalline SnO_2 was obtained. At the same time, with the increase of calcination temperature, the characterization diffraction peaks of SnO_2 became more and more sharp, indicating the particle size of SnO_2 increased. The average diameters of particles treated at different temperature were calculated by using Scherrer's equation based on the XRD peak broadening analysis at the (1 1 0) peak and listed in Table 1.

Fig. 2 shows the XRD patterns of the Au/SnO_2 catalysts with different Au loading. In the XRD patterns of the samples with

Table 1
Mean particle size of tin dioxide treated at various temperatures

	T (K)				
	473	573	673	773	873
D_{110} (nm)	3.2	3.8	6.0	12.2	18.4

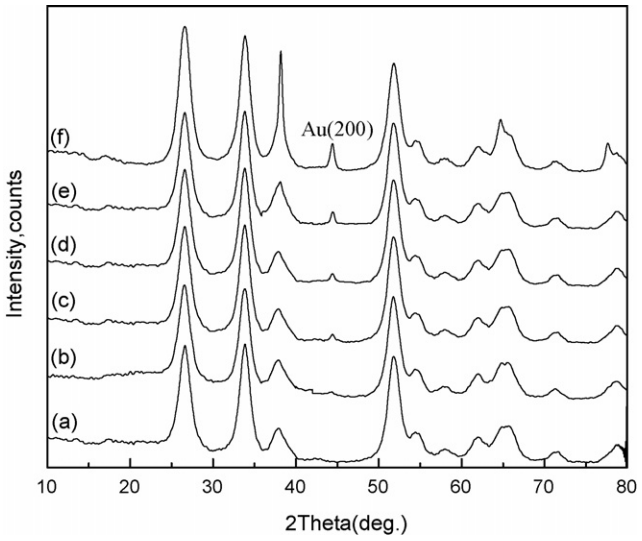

Fig. 2. XRD patterns of the Au/SnO_2 catalysts with different Au loading: 2.14 wt.% (a), 2.86 wt.% (b), 3.21 wt.% (c), 3.57 wt.% (d), 4.29 wt.% (e) and 5.00 wt.% (f).

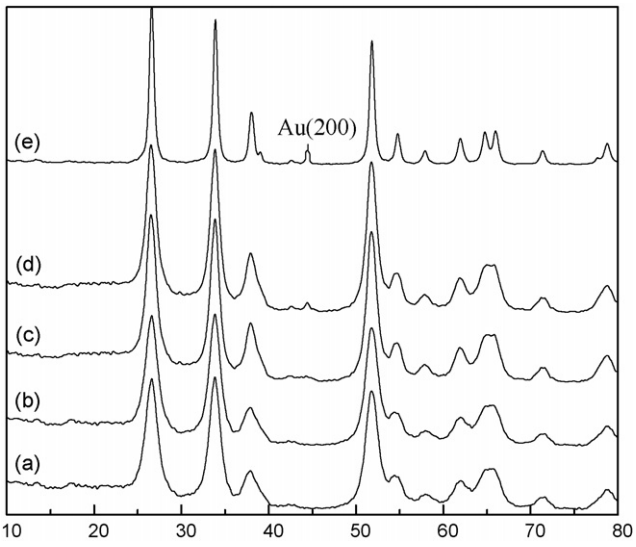

Fig. 3. XRD patterns of the SnO_2 support calcined at 673 K (a) and 1.43 wt.% Au/SnO_2 catalysts calcined at different temperatures: 473 K (b), 573 K (c), 673 K (d) and 773 K (e).

Au loading below 2.14 wt.%, no reflection peaks of gold were observed. This was probably due to the small particle size and low content of gold, and therefore its reflection peaks did not allow to be discriminated from the background. When the Au loading reached 2.86 wt.%, the weak Au (2 0 0) diffraction peak at $2\theta = 44.4^\circ$, related to the presence of metallic gold (JCPDS Card No. 04-0784), could be detected faintly. For the samples with Au loading above 3.21 wt.%, the Au (2 0 0) diffraction peak could be clearly observed. With the increase of Au loading, the Au (2 0 0) characterization diffraction peak became more significant and sharper, indicating the mean particle size of the gold in the Au/SnO_2 catalysts increased. The average size of gold particles calculated from the Au (2 0 0) reflection peak by using the Scherrer's equation was listed in Table 2.

Fig. 3 shows the XRD patterns of the 1.43 wt.% Au/SnO_2 catalysts (SnO_2 support calcined at 673 K for 3 h) calcined at different temperatures. In the XRD pattern of the sample calcined at 473 K almost no reflection peaks of gold were observed. This was probably due to the small particle size of gold, and therefore its reflection peaks did not allow to be discriminated from the background. For the sample calcined at 573 K, the weak Au (2 0 0) diffractions peak at $2\theta = 44.4^\circ$ could be detected faintly. At higher calcination temperature (673 K), the Au (2 0 0) diffraction peak could be clearly observed. With further increasing calcination temperature, the characterization peaks diffracted from the gold became more significant, indicating the gold particle size increased. The average size of gold particles, calculated from the Au (2 0 0) reflection peak by using the Scherrer's equation, was listed in Table 3, in which TEM results were also included.

HRTEM measurements (Fig. 4a) showed that tin dioxide was highly crystalline after calcination at 673 K. The selected area electron diffraction (SAED) pattern (inset in Fig. 4a) of the SnO_2 support distinctly exhibited four diffraction rings, which corresponded to the (1 1 0), (1 0 1), (2 1 1) and (1 1 2) planes of the tetragonal-phase SnO_2 with rutile structure, respectively. This was perfectly in agreement with the XRD analytical results, and indicated that the SnO_2 nanoparticles were well crystallized. It was also confirmed by energy-dispersive X-ray spectra (EDS; Fig. 4b) that there were not any impurities, indicating that chlorides were completely removed during washing.

Fig. 4c, d, f–h presented the bright-field images of the 1.43 wt.% Au/SnO_2 catalysts calcined at different temperatures. As shown in Fig. 4c, the gold nanoparticles were dispersed effectively on the surface of the SnO_2 nanoparticles after calcined at 473 K for 3 h and were not agglomerated. The gold nanoparticles had crystallite sizes between 2 and 4 nm. The energy-dispersive X-ray spectrum (Fig. 4e) confirmed the presence of Au element. It was also confirmed by EDS that there were not any impurities, indicating that chlorides were completely removed after washing. The interplanar spacing of the gold nanoparticle in HRTEM images (Fig. 4d) was ca. 0.24 nm, corresponding to the interplanar distance of the (1 1 1) plane of Au nanocrystal. The interference fringe of the (1 1 0) plane of inner

Table 2
Mean particle size of Au in the Au/SnO_2 catalysts with different Au loading

	Au loading (wt.%)				
	2.86	3.21	3.57	4.29	5.00
D_{200} (nm)	2.5	4.4	7.1	10.1	13.9

Table 3
Mean diameter of gold particles (D_{Au}) determined by XRD and TEM study for Au/SnO_2 catalysts calcined at different temperatures (T)

	T (K)			
	473	573	673	773
D_{Au} XRD (nm)	ND	ND	6.8	14.5
D_{Au} TEM (nm)	3	4.5	6	14.2

SnO_2 nanoparticles was clearly observed in the HRTEM image (Fig. 4d), demonstrating a good crystallinity and a high stability of SnO_2 nanoparticles after the decoration of Au nanoparticles. The HRTEM photograph of the samples calcined at 573 K, presented in Fig. 4f, also showed highly dispersed gold particles, and the small gold particles were also observed. The increase of the particle size of Au with increasing calcination temperature could be observed clearly, which confirmed the XRD results. The larger gold particles (10 nm) in the sample calcined at 673 K were occasionally found in the TEM (Fig. 4g). The TEM results in Fig. 4h showed gold particles in Au/SnO_2 sintered after calcined at 773 K, almost no gold particles with particle size <6 nm existed and the particle size lied between 6 and 20 nm. The mean diameters of Au particles in Au/SnO_2 catalysts were estimated by averaging diameters of more than 100 individual particles and listed in Table 3. It was clear that during the calcinations above 673 K of the catalysts the sintering of Au clusters would occur.

The full-range XPS spectra of the 1.43 wt.% Au/SnO_2 catalysts calcined at different temperatures were shown in Fig. 5. The XPS spectra revealed that the surface of samples contained gold, tin, oxygen and carbon elements. The absence of chlorine was a good indication of the effectiveness of the washing procedure. For the Au/SnO_2 catalyst with 1.43 wt.% Au loading, the nominal Au/Sn atom ratio was 0.011. However, the surface Au/Sn atom ratio of all samples in XPS was higher than 0.011, and the value of surface Au/Sn atom ratio decreased with the increase of calcination temperature. The Au/Sn atom ratio in XPS is tentatively used to represent the Au dispersion. This indicated that Au particles were well dispersed on the surface of SnO_2, and that Au particle size increased with the increase of the calcination temperature. The result was agreement with the XRD and TEM data.

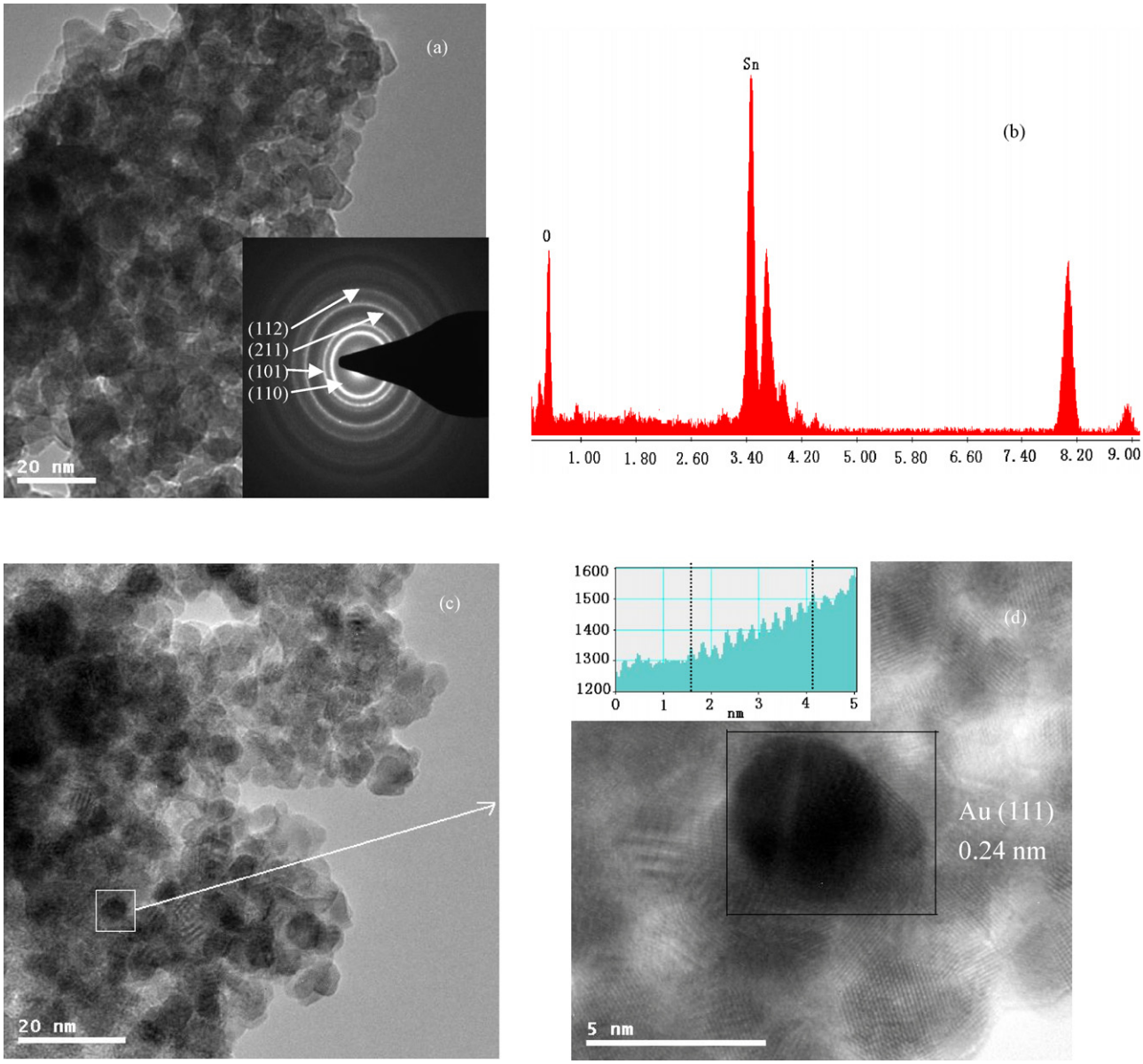

Fig. 4. HRTEM images of SnO_2 calcined at 673 K (a) and 1.43 wt.% Au/SnO_2 nanoparticles calcined at different temperatures: 473 K (c and d), 573 K (f), 673 K (g) and 773 K (h). (b and e) The EDS spectra of SnO_2 calcined at 673 K and Au/SnO_2 nanoparticles calcined at 473 K, respectively.

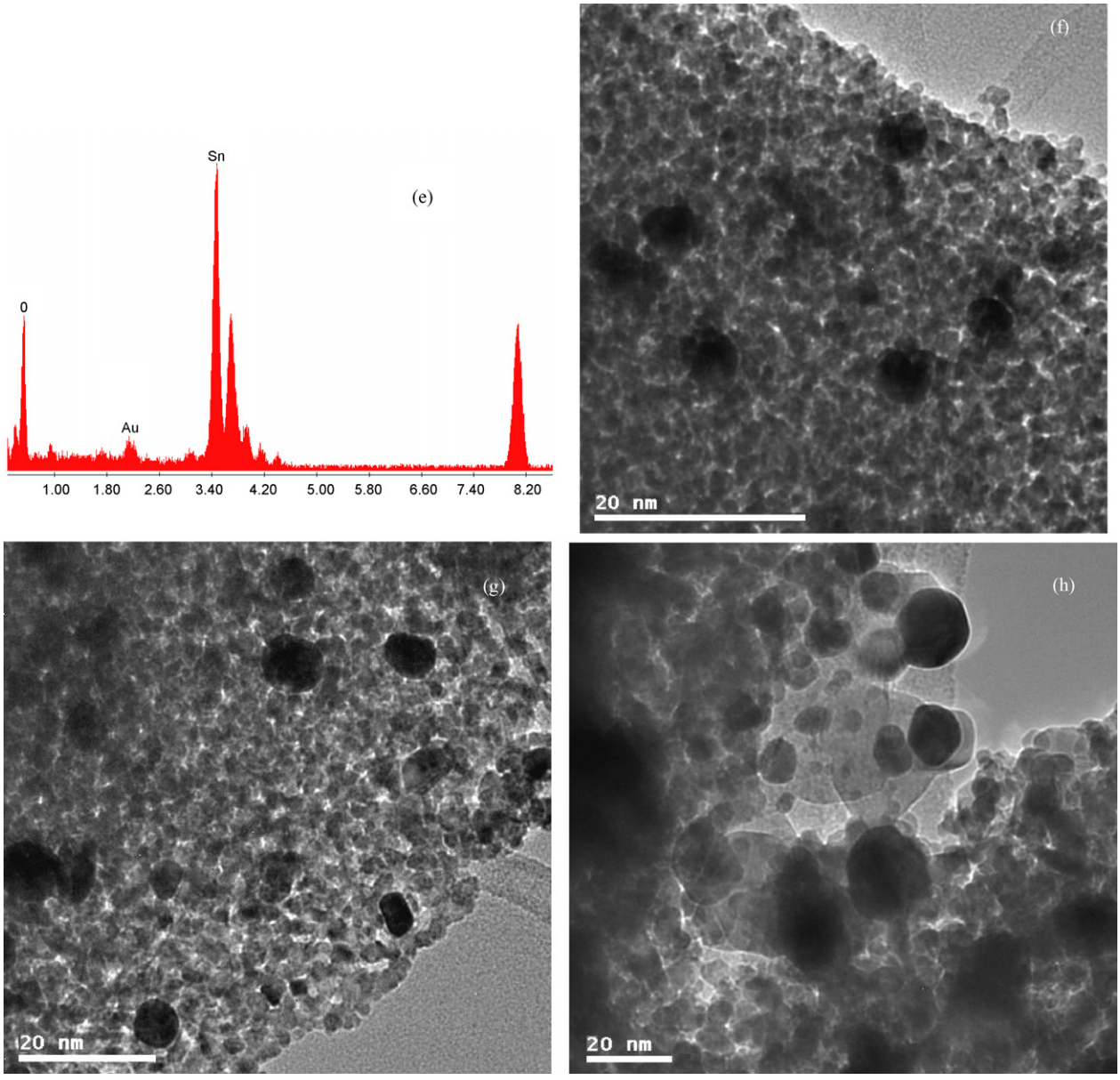

Fig. 4. (*Continued*).

Fig. 6 compared the XPS spectra in the Au 4f region of the1.43 wt.% Au/SnO_2 catalysts calcined at different temperatures. In all samples, the characteristic doublets of Au $4f_{7/2}$ and $4f_{5/2}$ peaks were observed. The two peaks for the uncalcined catalyst were at 85.3 and 88.9 eV, respectively, which were similar to those reported on Au^{3+} compounds [23]. Increasing calcination temperature, the Au $4f_{7/2}$ and $4f_{5/2}$ peaks became sharper and shifted to lower binding energy (84.2 and 87.8 eV) indicating an increase of the fraction of Au^0. For the sample calcined at 473 K, the two peaks were 84.4 and 88.1 eV, which were slightly larger than these of metallic state Au (84.2 and 87.8 eV) but smaller than these of oxidation state Au, indicating a mixture of oxidation state Au and metallic state Au. The samples calcined above 473 K showed that the Au $4f_{7/2}$ peak centered at 84.2 eV and Au $4f_{5/2}$ peak centered at 87.8 eV, which was characteristics of Au in a metallic state [24,25].

3.2. Catalytic performance

Fig. 7 shows the activity of 2.14 wt.% Au catalysts supported on different calcination temperature SnO_2 support with the Au catalysts calcined at 473 K for 3 h. For the Au/SnO_2 catalyst with the SnO_2 support calcined at 873 K, no obvious CO conversion was detected below 413 K reaction temperature. The Au/SnO_2 catalysts with the SnO_2 support calcined at 473 and 773 K were found not to be particularly active in CO oxidation. In fact, no 100% CO conversion was detected in the reaction temperature range of 283–413 K. The highest CO conversion over Au/SnO_2 catalyst with the SnO_2 support calcined at 473 K was lower than Au/SnO_2 catalyst with the SnO_2 support calcined at 773 K. The Au/SnO_2 catalysts with the SnO_2 support calcined at 573 and 673 K clearly exhibited a better performance than other catalysts, and the Au/SnO_2 catalyst with the SnO_2 support calcined

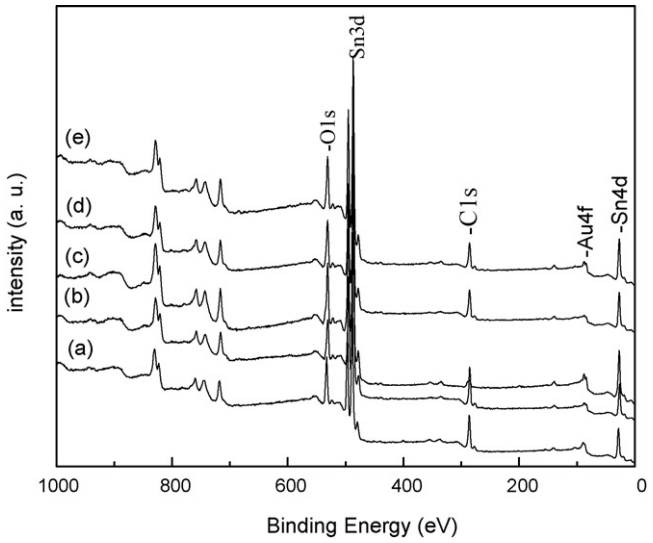

Fig. 5. Full-range XPS spectra of the 1.43 wt.% Au/SnO_2 catalysts calcined at different temperatures: 298 K (a), 423 K (b), 473 K (c), 573 K (d) and 673 K (e).

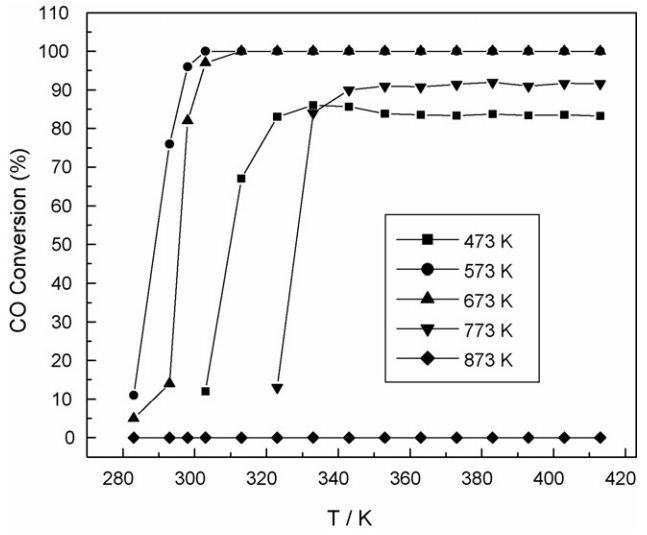

Fig. 7. Influence of calcination temperature of SnO_2 supports on the activity of Au/SnO_2 catalysts for CO oxidation.

at 573 K was more active than the Au/SnO_2 catalyst with the SnO_2 support calcined at 673 K. This indicated that the calcination temperature of SnO_2 support had an evidently influence on catalytic activity of Au/SnO_2 catalysts, and SnO_2 samples calcined at 573 and 673 K were suitable support materials for the Au/SnO_2 catalysts. The XRD results (Fig. 3) indicated that crystalline structure tended towards integrity and the particle size of SnO_2 increased with the increase of calcination temperature. The interaction between gold and support is of substantial importance in the case of CO oxidation. The smaller SnO_2 nanoparticles may supply more active sites and contribute to the strong interaction between gold and nanocrystalline SnO_2. Therefore, the catalytic activity of Au/SnO_2 (573 K) was better as compared to that of Au/SnO_2 (>673 K). On the other hand, the degree of crystallinity of the support also brought markedly influence on the catalytic activity. Therefore, the Au/SnO_2 (573 K) catalyst was more active than the Au/SnO_2 (473 K). We suggested that the catalytic activity of Au/SnO_2 catalysts was related to both the particle size and the degree of crystallinity of tin dioxide support.

Figs. 8 and 9 show the relationship between the activity and the Au loading in Au/SnO_2 catalysts. The loading of gold in the Au/SnO_2 catalysts markedly influenced the catalytic activity. The optimum Au loading was 2.86 wt.%, which had an appreciably high catalytic activity [the temperature of 100% CO conversion ($T_{100\%}$) was 303 K]. When the Au loading was below 2.86 wt.%, $T_{100\%}$ decreased with the increase of the gold loading. On the other hand, when the Au loading was above 2.86 wt.%, $T_{100\%}$ increased with the increase of the gold loading. This indicated that a proper Au loading was necessary to gain high activity

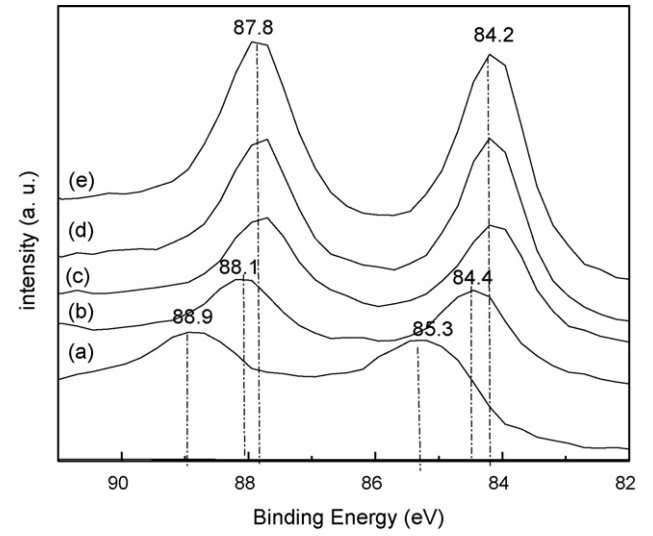

Fig. 6. XPS spectra of Au 4f region for 1.43 wt.%Au/SnO_2 catalysts calcined at different temperatures: 298 K (a), 423 K (b), 473 K (c), 573 K (d) and 673 K (e).

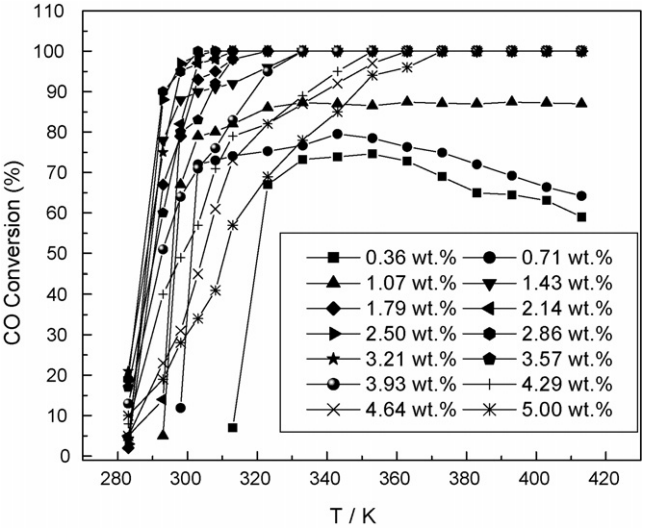

Fig. 8. Influence of Au loading on the activity of Au/SnO_2 catalysts for CO oxidation.

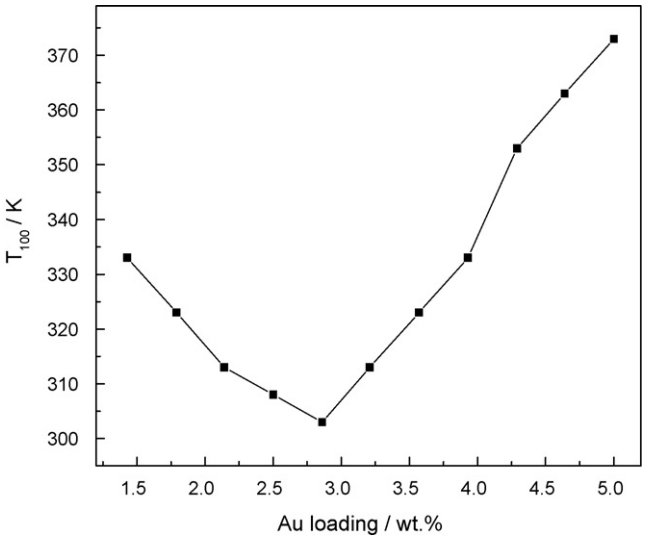

Fig. 9. Influence of Au loading on 100% conversion temperature ($T_{100\%}$) of CO over Au/SnO_2 catalysts.

Au catalyst. From the XRD results (Fig. 2 and Table 2), we could see that when the Au loading was above 2.86 wt.%, the average size of gold particles significantly increased with the increase of Au loading, which could be an important factor resulted in the decrease of catalytic activity.

Fig. 10 shows the influence of the calcination temperature of 1.43 wt.% Au/SnO_2 catalysts on the catalytic activity. The uncalcined material had no activity when the reaction temperature was below 423 K. The catalyst pretreated at 423 K had already had certain activity, which could oxidize CO to CO_2 at 323 K, and the $T_{100\%}$ was 383 K. With the increase of calcination temperature, the catalytic activity increased. The catalyst calcined at 473 K showed the best catalytic performance ($T_{100\%}$ was 333 K). When the calcination temperature was above 573 K, with the increase of calcination temperature, a decrease in the catalytic activity could be observed. The sample calcined at 773 K displayed no

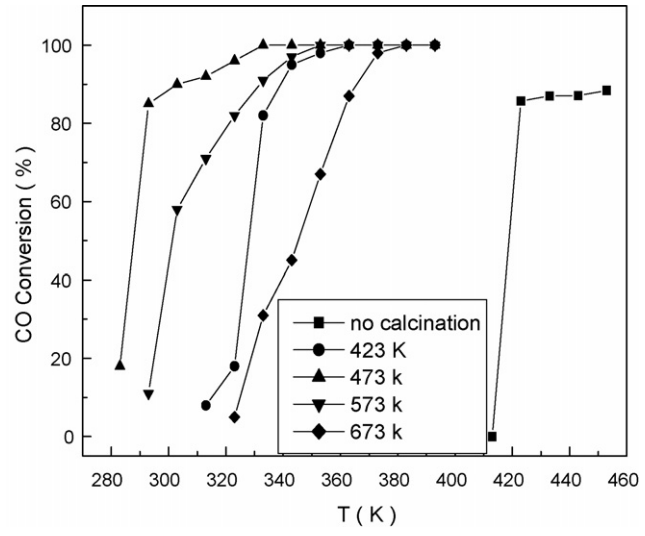

Fig. 10. Influence of calcination temperature of Au/SnO_2 catalysts on catalytic activity of CO oxidation.

activity when reaction temperature was below 393 K. The results reported in the present paper showed that the catalytic behavior of the Au/SnO_2 system was remarkably influenced by the thermal pretreatment of the catalyst. A calcination pretreatment was necessary to activate the catalyst, but the activity decreased rapidly in high pretreatment temperature above 673 K. The XPS analyses results showed for the sample uncalcined and calcined at 423 K, the fraction of Au^0 was lower than the samples calcined above 473 K. Increasing the calcination temperature, the fraction of Au^0 increased. The samples calcined above 473 K showed the Au $4f_{7/2}$ peak centered at 84.2 eV and Au $4f_{5/2}$ peak centered at 87.8 eV, which was characteristics of Au^0. This indicated that the fraction of Au^0 markedly influenced the catalytic activity, which resulted in the catalyst calcined at 473 K was more active than the catalysts uncalcined and calcined at 423 K. Higher calcination temperature than 673 K result in the formation of bigger (>10 nm) Au agglomerates, and these catalysts demonstrated lower activity as compared to the ones containing mostly small Au nanoparticles. It was clear that during the calcination above 673 K the sintering of Au clusters of the catalysts would occur, which resulted in a rapid decrease in the catalytic activity after high pretreatment temperature above 673 K. From the XRD and TEM results, we suggested that the increasing size of the gold particles was responsible for the decreasing catalytic activity at higher calcination temperature.

4. Conclusions

The calcination temperature of SnO_2 support had an evidently influence on catalytic activity of Au/SnO_2 catalysts, and SnO_2 samples calcined at 573 and 673 K were suitable support materials for the Au/SnO_2 catalysts. From the XRD results, it was suggested that the catalytic activity of Au/SnO_2 catalysts were related to both the particle size and the degree of crystallinity of tin dioxide support.

The loading of gold in the Au/SnO_2 catalysts markedly influenced the catalytic activity. In all investigated Au/SnO_2 catalysts with different Au loading from 0.36 to 5.00 wt.%, the catalytic activity of the catalyst with 2.86 wt.% Au loading was the highest. When the Au loading was below 2.86 wt.%, the catalytic activity increased with the increase of the Au loading. On the other hand, when the Au loading was above 2.86 wt.%, the catalytic activity decreased with the increase of the Au loading.

The results reported in the present paper showed that the catalytic behavior of the Au/SnO_2 system was remarkably influenced by the thermal pretreatment of the catalyst. The optimum calcination temperature of the Au/SnO_2 catalysts was 473 K. A calcination pretreatment was necessary to activate the catalyst, but the activity decreased rapidly when the pretreatment temperature was higher than 673 K. The XPS analyses results showed that the fraction of metallic state Au markedly influenced the catalytic activity, which resulted in the catalyst calcined at 473 K was more active than the catalysts uncalcined and calcined at 423 K. From the XRD and TEM results, we suggested that the increasing size of the gold particles was responsible for the decreasing catalytic activity at higher calcination temperature.

References

[1] T. Salama, R. Ohnishi, T. Shido, M. Ichikawa, J. Catal. 162 (1996) 169.
[2] T. Salama, R. Ohnishi, T. Shido, M. Ichikawa, Chem. Commun. (1997) 105.
[3] T. Hayashi, K. Tanaka, M. Haruta, J. Catal. 178 (1998) 566.
[4] E.E. Stangland, K.B. Stavens, R.P. Andres, W.N. Delgass, Stud. Surf. Sci. Catal. 130 (2000) 827.
[5] M. Haruta, Catal. Today 36 (1997) 153.
[6] A. Baiker, M. Maciejewski, S. Tagliaferri, J. Catal. 151 (1995) 407.
[7] M.A. Bollinger, M.A. Vannice, Appl. Catal. B 8 (1996) 417.
[8] F.E. Wagner, S. Galvagno, C. Milone, A.M. Visco, L. Stievano, S. Calogero, J. Chem. Soc. Faraday Trans. 93 (1997) 3403.
[9] Y. Yuan, K. Asakura, H. Wan, K. Tsai, Y. Iwasawa, Chem. Lett. (1996) 755.
[10] Y. Yuan, A.P. Kozlova, K. Asakura, H. Wan, K. Tsai, Y. Iwasawa, J. Catal. 170 (1997) 191.
[11] A.P. Kozlova, S. Sugiyama, A.I. Kozlov, K. Asakura, Y. Iwasawa, J. Catal. 176 (1998) 426.
[12] A.I. Kozlov, A.P. Kozlova, H.C. Liu, Y. Iwasawa, Appl. Catal. A 182 (1999) 9.
[13] G.J. Hutchings, M.R.H. Siddigui, A. Burrows, C.J. Kiely, R. Whyman, J. Chem. Soc. Faraday Trans. 93 (1997) 187.
[14] G.B. Hoflund, S.D. Gardner, D.R. chryer, B.T. Upchurch, E. Jielin, Appl. Catal. B 6 (1995) 117.
[15] M. Haruta, T. Kobayashi, H. Sano, N. Yamada, Chem. Lett. (1987) 405.
[16] M. Haruta, N. Yamada, T. Kobayashi, S. Iijima, J. Catal. 115 (1989) 301.
[17] M. Haruta, S. Tsubota, T. Kobayashi, H. Kageyama, M.J. Genet, B. Delmon, J. Catal. 144 (1993) 175.
[18] M. Haruta, T. Kobayashi, H. Sano, N. Yamada, Chem. Lett. (1987) 405.
[19] P.N. Santhosh, H.S. Potde, S.K. Date, J. Mater. Res. 12 (1997) 326.
[20] R.D. Goodman, A.G. Menke, Solar Energy 17 (1995) 202.
[21] O. Wurzinger, G. Reinhardt, Sens. Actuators B 103 (2004) 104.
[22] S. Wang, J. Huang, L. Geng, B. Zhu, X. Wang, S. Wu, S. Zhang, W. Huang, Catal. Lett. 108 (1–2) (2006) 97.
[23] E.D. Park, J.S. Lee, J. Catal. 186 (1999) 1.
[24] D. van der Putten, R. Zanoni, J. Electron. Spectrosc. Relat. Phenom. 76 (1995) 741.
[25] J. Coulthard, S. Degen, Y.-J. Zhu, T.K. Sham, Can. J. Chem. 76 (1998) 1707.